Han et al. *Zool. Res.* 2025, 46(1): 41−53
https://doi.org/10.24272/j.issn.2095-8137.2024.257
https://cstr.cn/32248.14.zr.2024.257

ZR | Zoological Research

Article Open Access

Novel mouse model of Alzheimer's disease exhibits pathology through synergistic interactions among amyloid-β, tau, and reactive astrogliosis

Young-Eun Han[1,#], Sunhwa Lim[1,#], Seung Eun Lee[2], Min-Ho Nam[1], Soo-Jin Oh[1,*]

[1] *Brain Science Institute*, *Korea Institute of Science and Technology (KIST)*, *Seoul* 02792, *Republic of Korea*

[2] *Research Animal Resources Center*, *Korea Institute of Science and Technology (KIST)*, *Seoul* 02792, *Republic of Korea*

ABSTRACT

Alzheimer's disease (AD) is a progressive neurodegenerative disorder characterized by cognitive impairment and distinct neuropathological features, including amyloid-β plaques, neurofibrillary tangles, and reactive astrogliosis. Developing effective diagnostic, preventative, and therapeutic strategies for AD necessitates the establishment of animal models that accurately recapitulate the pathophysiological processes of the disease. Existing transgenic mouse models have significantly contributed to understanding AD pathology but often fail to replicate the complexity of human AD. Additionally, these models are limited in their ability to elucidate the interplay among amyloid-β plaques, neurofibrillary tangles, and reactive astrogliosis due to the absence of spatially and temporally specific genetic manipulation. In this study, we introduce a novel AD mouse model (APP/PS1-TauP301L-Adeno mice) designed to rapidly induce pathological symptoms and enhance understanding of AD mechanisms. Neurofibrillary tangles and severe reactive astrogliosis were induced by injecting AAV_{DJ}-EF1a-hTauP301L-EGFP and Adeno-GFAP-GFP viruses into the hippocampi of 5-month-old APP/PS1 mice. Three months post-injection, these mice exhibited pronounced astrogliosis, substantial amyloid-β plaque accumulation, extensive neurofibrillary tangles, accelerated neuronal loss, elevated astrocytic GABA levels, and significant spatial memory deficits. Notably, these pathological features were less severe in AAV-TauP301L-expressing APP/PS1 mice without augmented reactive astrogliosis. These findings indicate an exacerbating role of severe reactive astrogliosis in amyloid-β plaque and neurofibrillary tangle-associated pathology. The APP/PS1-TauP301L-Adeno mouse model provides a valuable tool for advancing therapeutic research aimed at mitigating the progression of AD.

Keywords: Alzheimer's disease mouse model; Neurofibrillary tangles; Amyloid-β plaques; Reactive astrogliosis; Alzheimer's disease pathology

INTRODUCTION

Alzheimer's disease (AD) is a neurodegenerative disorder and the primary cause of dementia, characterized by progressive cognitive decline, neuronal loss, and hippocampal atrophy. The pathological features of AD include extracellular amyloid-β (Aβ) plaques and intracellular neurofibrillary tangles (NFTs), composed of Aβ peptide and hyperphosphorylated tau (p-tau) protein, respectively (Querfurth & Laferla, 2010). Mutations in genes associated with the amyloid precursor protein (APP) processing pathway, particularly in familial AD, accelerate amyloid pathology through increased Aβ42 aggregation, leading to neuronal degeneration and memory deficits (Selkoe & Kopan, 2003). Additionally, tau, encoded by the microtubule-associated protein tau (*MAPT*) gene, dissociates from microtubules, undergoes hyperphosphorylation, and forms pathological tau, driving neuronal cell death and cognitive deficits (Di et al., 2016).

In addition to Aβ plaques and NFTs, growing evidence suggests that reactive astrogliosis severity is also associated with AD progression (Chun et al., 2020; Ingelsson et al., 2004). In the AD brain, astrocytes proximal to Aβ plaques or NFTs undergo morphological, molecular, and functional alterations that drive reactive astrogliosis. Key characteristics of reactive astrocytes include the up-regulation of intermediate filaments, such as glial fibrillary acidic protein (GFAP) and

This is an open-access article distributed under the terms of the Creative Commons Attribution Non-Commercial License (http://creativecommons.org/licenses/by-nc/4.0/), which permits unrestricted non-commercial use, distribution, and reproduction in any medium, provided the original work is properly cited.

Copyright ©2025 Editorial Office of Zoological Research, Kunming Institute of Zoology, Chinese Academy of Sciences

Received: 06 August 2024; Accepted: 11 November 2024; Online: 12 November 2024

Foundation items: This study was supported by the National Research Foundation of Korea (NRF) funded by the Ministry of Science, ICT & Future Planning (2022R1A2C2006229, 2022R1A6A3A01086868), Korea Dementia Research Project through the Korea Dementia Research Center (KDRC) funded by the Ministry of Health & Welfare and Ministry of Science and ICT, Republic of Korea (RS-2024-00345328), and KIST Institutional Grant (2E32851)

[#]Authors contributed equally to this work

*Corresponding author, E-mail: osj@kist.re.kr

vimentin, as well as the development of hypertrophic processes (Bardehle et al., 2013; Jiwaji et al., 2022; Jo et al., 2014; Kato et al., 1998; Simpson et al., 2010; Yamada et al., 1992). In addition to morphological changes, reactive astrocytes also exhibit molecular dysregulation, including aberrant GABA synthesis and release, which suppress neuronal activity and contribute to memory deficits in AD (Chun et al., 2020; Jo et al., 2014; Nam et al., 2023). Brain insults, including injury, inflammation, and infection, can trigger widespread astrocyte reactivity. Notably, intracerebral injection of high-titer adenovirus, such as Adeno-GFAP-GFP, into the hippocampus of APP/PS1 mice has been shown to induce severe neuroinflammation and reactive astrogliosis, exacerbating neurodegeneration and cognitive deficits (Chun et al., 2020; Nam et al., 2020; Woo et al., 2017). Compared to adeno-associated virus (AAV), adenovirus elicits a stronger inflammatory response (Shirley et al., 2020) and is suitable for inducing reactive astrocytes through astrocyte-specific infection. Additionally, adenovirus-induced reactive astrogliosis has been shown to exacerbate pathology in Parkinson's disease models (An et al., 2021), suggesting that reactive astrogliosis may represent a common pathological mechanism in various neurodegenerative diseases. Based on these findings, we propose that the artificial induction of reactive astrogliosis, in conjunction with Aβ plaques and p-tau pathology, may exacerbate the pathological features of AD, providing a valuable and efficient mouse model for AD research.

Effective animal models that reflect the progressive neuropathology and cognitive decline of AD are essential for expanding our understanding of its molecular pathology and developing therapeutic approaches. While widely utilized transgenic mouse models, including APP/PS1, 5xFAD, and 3xTg, have provided valuable insights into AD, they fail to replicate key AD features. For example, APP/PS1 and 5xFAD mouse models do not exhibit neuronal loss or NFTs even after one year (Jackson et al., 2016). Similarly, 3xTg mouse models show limited accumulation of Aβ plaques and NFTs even after two years, and their pathology remains less severe than what is typically observed in human AD (Drummond & Wisniewski, 2017). Moreover, these models lack the temporal and spatial precision necessary to understand the complex interplay among Aβ plaques, NFTs, and reactive astrogliosis. These limitations highlight the need for virus-based AD mouse models capable of inducing pathology with spatial and temporal specificity.

To address these limitations, we developed a novel AD mouse model (APP/PS1-TauP301L-Adeno mice). The model was established by injecting AAV_{DJ}-EF1α-hP301L-EGFP (AAV-TauP301L) and Adeno-GFAP-GFP viruses into the hippocampus of APP/PS1 mice. This approach generated a comprehensive AD phenotype marked by severe reactive astrogliosis, extensive NFT formation, exacerbated Aβ plaque deposition, and substantial neurodegeneration, closely mirroring human AD pathology. Collectively, these pathological markers contributed to pronounced hippocampus-dependent memory impairments. Using this model, we demonstrated that the induction of reactive astrogliosis via Adeno-GFAP-GFP infection, in the presence of toxic molecules such as Aβ and p-Tau, markedly amplified the aggregation of Aβ plaques and NFTs, ultimately exacerbating pathological symptoms of AD, such as neuronal loss and memory deficits. The APP/PS1-TauP301L-Adeno model thus provides a robust platform for investigating the interrelationship between key AD pathologies and should serve as a valuable tool for developing and testing novel therapeutic strategies in AD.

MATERIALS AND METHODS

Animals

Five-month-old hemizygous APPswe/PSEN1dE9 (APP/PS1) mice on a C57BL/6;C3H genetic background (Jackson Laboratory, #004462, USA) were used to assess the effects of increased tau pathology and activation on Aβ. Age-matched non-transgenic littermates were used as wild-type (WT) controls. Both male and female transgenic and WT mice were included in the study. Mice were maintained on a 12-h light-dark cycle with free access to food and water. All animal care and handling procedures were performed under the Institutional Animal Care and Use Committee (IACUC) guidelines of the Korea Institute of Science and Technology (KIST) (Approval number: KIST-IACUC-2019-051).

Viral vector design and production

All AAV and adenoviral vector plasmids were generated by the KIST Virus Facility. For AAV-based TauP301L expression, the TauP301L sequence from pRK5-EGFP-TauP301L (Addgene, #46908, USA) was inserted into the AAV-EF1α-EGFP vector backbone (Addgene, #60058, USA) at the KpnI and NcoI restriction sites using infusion cloning (Clontech, #639649, USA). The control vector, AAV-EF1α-EGFP (Addgene, #60058, USA), was similarly prepared. The resulting viral vectors were pseudotyped, with the transgene of interest flanked by inverted terminal repeats of the AAV2 and packaged in AAV-DJ capsids. The AAV-DJ capsids were engineered using DNA family shuffling technology, creating a hybrid capsid from eight standard AAV serotypes. Recombinant AAV (rAAV) vector production required four plasmids: AAV-DJ-serotype, AAV vector transfer plasmid, plasmid encoding rep and serotype-specific cap, and plasmid encoding adenoviral helper sequences. All vectors were purified via iodixanol gradients by the KIST Virus Facility. To induce reactive astrogliosis, we utilized an adenoviral vector (Adeno-GFAP-GFP) driven by the gfaABC1D promoter, a truncated version of the human GFAP promoter optimized for high astrocyte specificity (Lee et al., 2008). The AAV_{DJ}-EF1α-EGFP and AAD_{DJ}-EF1α-hTauP301L-EGFP titers were 1.26×10^{13} GC/mL, while the Adeno-GFAP-GFP titer was 2.25×10^{11} GC/mL.

Stereotaxic surgery

To achieve neuronal expression of human P301L-mutant tau, 5-month-old APP/PS1 transgenic mice and their littermate controls were anesthetized via isoflurane and secured in a stereotaxic frame (David Kopf Instruments, USA). After craniotomy, a 0.5 mm bore hole was drilled on each side of the skull using a drill handpiece (Komet Dental, Germany). Viral suspensions were microinjected using a 33-gauge blunt needle connected to a 25 μL Hamilton syringe and an automated microsyringe pump (kdScientific, USA). AAV_{DJ}-EF1α-EGFP (Control), AAV_{DJ}-EF1α-hTauP301L-EGFP (TauP301L), or Adeno-GFAP-GFP (adenovirus) was bilaterally injected into the CA1 region and dentate gyrus (DG) of the hippocampus based on the following coordinates: AP=−1.96, ML=±1.5, and DV=−1.7 for the DG; AP=−1.96, ML=±1.5, and DV=−1.2 for the CA1 to the dura surface. The

AAV-control, AAV-TauP301L, and Adeno-GFAP-GFP viruses were diluted 1:1 and a total volume of 1.5 μL was injected into each region at a rate of 0.2 μL/min. For co-injections of AAV-TauP301L and Adeno-GFAP-GFP, equal volumes of each virus (0.75 μL) were mixed and diluted with 0.5 μL of sterilized saline, with a total volume of 2.0 μL injected into each region at a rate of 0.2 μL/min. Before withdrawal, the needle was kept in position for an additional 5 min to prevent leakage of the infused solution. The injection site was then sutured, and the mice were maintained on a heating pad until fully recovered before being returned to their home cages.

Behavioral analyses

To assess cognitive and memory changes at the behavioral level, APP/PS1 transgenic mice (5 months old) and non-transgenic WT littermates (5 months old), with or without TauP301L and adenovirus injections, were assessed at 3 months post-injection. Behavioral tests were conducted sequentially, including the open field test, novel object recognition test, Y-maze test, and passive avoidance test. Before testing, all mice were extensively handled and habituated to an empty testing apparatus for 10 min daily over six consecutive days. Mice were also habituated to the testing room for 30 min before each test. Sex ratios of mice were balanced across experimental groups to minimize variability.

Open field test: Locomotor activity and anxiety-related behaviors were evaluated using the open field test. Testing was performed in an open field arena measuring 40 cm×40 cm. Testing commenced at least 24 h after the final habituation session. Mice remained in their home cages until testing and were transported to the arena immediately prior to the test. Mice were individually placed in the center of the arena and allowed to explore freely for 30 min. The total distance traveled, as well as the time and distance spent in the center versus the perimeter, were recorded using Noldus tracking software (EthoVision XT, 8.5, USA).

Novel object recognition (NOR) test: Recognition memory was evaluated using the NOR test. To prevent navigation-related behaviors from interfering with object interaction, each mouse underwent a 30 min open field training session 24 h before the test. During the familiarization phase, each mouse was placed in a 40 cm×40 cm arena containing two identical objects fixed on stationary bases positioned on opposite sides. The mice were allowed to explore the objects for 30 min before being returned to their home cages (familiarization phase). After 1 h, one of the familiar objects was replaced with a novel object, each mouse was reintroduced to the arena and allowed to explore both the familiar and novel objects for 15 min (testing phase). All experiments were videotaped, and the time spent oriented towards the objects was manually scored using the EthoVision manual scoring system. Interaction with an object was defined as the time spent exploring it within a distance of 1.5 times the size of the object during the observation period. The discrimination ratio was defined as the time spent investigating the novel object divided by the time spent investigating both the novel and familiar objects (total time of exploratory behavior). The arena and all objects were cleaned with 70% ethanol between trials to eliminate olfactory cues.

Y-maze: To evaluate short-term spatial recognition working memory, mice were placed at the end of the B arm of a Y-maze and allowed to explore freely for 8 min. The Y-maze consisted of three arms, each 40 cm long, 4 cm wide, and 16 cm high, arranged at 120° angles. The maze, constructed from gray polyvinyl plastic, included posters on the walls to serve as spatial cues. After the exploration phase, each mouse was returned to its home cage for a 30 min interval. The maze was cleaned with 70% ethanol and dried before each trial to eliminate olfactory cues. During the test, overhead video recording was used to monitor behavior. Spatial working memory performance was assessed based on the proportion of alternations, defined as the number of arm entries in which the mouse selected a different arm from the previous two consecutive entries, relative to the total number of arm entries.

Passive avoidance test: The passive avoidance test was performed to measure long-term memory using a two-compartment apparatus consisting of light and dark chambers connected by a sliding door. During the acquisition trial on the first day, each mouse was placed in the light chamber and allowed to explore for 60 s, with the door separating the two spaces raised. When the mouse placed its paws in the dark chamber, the door was closed to prevent the mouse from returning to the light side and a 0.4 mA electrical shock was delivered through the metal grid for 2 s. Following the shock, the mouse was removed from the apparatus and returned to its home cage. The following day, retention was assessed by placing the mouse back into the light chamber. The sliding door was opened, and the latency to enter the dark chamber was recorded. No electrical stimulation was applied during the retention trial. The cut-off time for both the acquisition and retention trials was set to 600 s.

Immunohistochemical analysis

Mice were anesthetized with 2% avertin (20 μg/g, intraperitoneally) (Sigma-Aldrich, #T48402, USA) 13 weeks after virus injection. The anesthetized mice were transcardially perfused with phosphate-buffered saline (PBS, pH 7.4) and 4% paraformaldehyde in PBS. After perfusion, tissues were immediately removed and post-fixed for 12 h in the same fixative, followed by dehydration in 30% sucrose until they sank. Brains were coronally sectioned on a freezing microtome (Thermo Scientific, USA) at 30 μm thickness.

The blocking of non-specific binding sites was performed by incubating the sections in 0.1 mol/L PBS containing 0.3% Triton X-100 (Sigma, #T8787, USA), 2% goat serum (Abcam, ab7481, USA), and 2% donkey serum (Genetex, GTX27475, USA) for 2 h at room temperature (RT). Primary antibodies were prepared in blocking buffer and applied overnight at 4°C. After washing three times (5 min each) in 0.1 mol/L PBS, the brain slices were incubated in appropriate secondary antibodies (Jackson Laboratory) for 1.5 h at RT. The sections were again washed three times in 0.1 mol/L PBS and mounted in fluorescent mounting medium (Agilent Dako, S3023, USA). A series of fluorescent images were taken using an A1 Nikon confocal microscope. Z stack projections were made from serial images in 3 μm steps. Any alterations in brightness or contrast were equally applied to the entire image set. IMARIS software (Bitplane, UK) was used to view the three-dimensional (3D) reconstruction of all z-stacks.

Brain sections were stained with chicken anti-GFAP (1:500, MERCK, ab5541, USA), mouse anti-phosphorylated tau AT8 (pSer202 and pThr205; 1:200, Thermo Fisher Scientific, MN1020, USA), rabbit anti-phosphorylated human tau S199 (pSer199; Abcam, ab81268, USA), rabbit anti-neurofibrillary tangle (1:200, MERCK, ab1518, USA), rabbit anti-beta amyloid (1:500, Abcam, ab2539, USA), and guinea pig anti-

NeuN (MERCK, ABN90P, USA).

For NFT staining, sections were incubated with 3% hydrogen peroxide (H_2O_2) in PBS for 10 min at RT, then washed three times in PBS for 15 min. Non-specific binding sites were blocked by incubating the sections in 3% normal goat serum (Life Technologies, NC2459021, USA) and 3% Triton X-100 in PBS for 1 h at RT. The sections were then incubated overnight at 4℃ with primary antibodies against NFT (1:400, MERCK, ab1518, USA). After three washes in PBS, a biotinylated goat anti-rabbit (Vector Laboratories, BP-1000-1.5, USA) secondary antibody diluted 1/200 in PBS was applied for 2 h at RT. Following the manufacturer's instructions, a Vectastain ABC Elite Kit (Vector Laboratories, PK6101, USA) was used for peroxidase detection. Sections were washed and developed with 3,3'-diaminobenzidine (DAB, Sigma Aldrich, USA) plus H_2O_2 in Tris-buffered saline (TBS). The DAB-stained sections were mounted on microscopic slides, air-dried, and coverslipped. Images were obtained using an Olympus IX50 microscope with a 2× or 4× objective. Quantitative analyses were performed using ImageJ software to measure mean optical density.

Thioflavin-S staining

For thioflavin-S staining, frozen brain sections were incubated in 1 mmol/L thioflavin-S (Sigma Aldrich, USA) 50% ethanol for 8 min at RT, then washed twice in 80% ethanol for 5 min and twice in PBS for 10 min. Images were taken using an Olympus IX50 microscope (Japan) with a green fluorescence protein (GFP) filter set. The region of interest (ROI) (mm^2) in the cortex was measured using ImageJ software (NIH, USA). Counting was performed using a low-magnification objective lens (×2) and images were quantified as the number of plaques in the cortex. Data quantification was conducted via surface rendering of Aβ plaques using IMARIS (Bitplane, UK).

Image quantification

Quantitative analysis of confocal microscopic images was performed using IMARIS software. The ROI was determined as the 3D structure of the GFP-positive region using a "surface object" generated using a 0.312 μm diameter. Smaller, adjacent neurons were separated into multiple objects using the "split touching objects" function with an estimated 6 μm diameter. Thus, large puncta were potentially separated into several individual neurons. Average intensity of the pixels of different wavelengths (405 nm, 594 nm, and 647 nm) was measured by masking them with a GFP-positive cell. At least four mice per group were sacrificed after behavioral experiments, and 2–3 slices per mouse were stained and analyzed for quantification. Sholl analysis was performed using maximal projection images of GFAP signals. The Neuroanatomy Sholl analysis plugin in ImageJ was used to automatically generate consecutive concentric circles at 10 μm intervals, centered on the DAPI-stained nucleus and extending to the furthest reach of the astrocytic process. Subsequently, the sum of all intercepts of GFAP processes in each circle was quantified.

Monoamine oxidase-B (MAO-B) activity assay

Mice were anesthetized with avertin (tribromoethanol) via intraperitoneal injection and transcardially perfused with saline. Brain tissue was removed from six mouse groups. Different regions, including the hippocampus and cortex, were dissected separately under cold conditions. Fresh tissues from each mouse were homogenized in lysis buffer (250 mmol/L sucrose, 2 mmol/L HEPES (pH 7.4), 0.1 mmol/L EGTA), and centrifuged at 570 ×*g* for 10 min at 4°C to remove large debris. The supernatants were collected and centrifuged at 14 290 ×*g* for 10 min at 4°C to obtain a mitochondrial-rich fraction. The pellet was resuspended in PBS, and MAO-B activity was measured using 20 μg in each well. MAO-B enzymatic activity was measured using an Amplex Red Monoamine Oxidase Assay Kit (ThermoFisher Scientific. #A12214, USA), following the manufacturer's instructions. MAO-B was reacted at 37°C for 30 min with or without adding selegiline, a MAO-B inhibitor, then reacted with benzylamine, a MAO-B substrate. H_2O_2 production resulting from MAO-B activity was assessed using the colorimetric change of the Amplex Red reagent after 2 h of enzymatic reaction. The color change was quantified by measuring absorbance at 570 nm using an Infinite M200 PRO microplate reader (TECAN, Switzerland).

Statistical analysis

Results were presented as mean±standard error of the mean (SEM). All data were analyzed statistically using Prism v.9.0 (GraphPad Software, USA). Statistical significance was determined by either one-way or two-way analysis of variance (ANOVA), as reported in each figure legend. One-way ANOVA with Tukey's multiple comparison test was conducted to compare multiple groups. Two-way ANOVA followed by Bonferroni's multiple comparison test was used to assess changes under different conditions across multiple groups. Differences were considered significant at *: $P<0.05$, **: $P<0.01$, ***: $P<0.001$, ****: $P<0.0001$ (ns, not significant). All raw data are shown as dot plots on each graph. The corresponding figure legend or graph describes the number of animals used. Experimental groups were balanced regarding animal age, sex, and weight.

RESULTS

Rapid accumulation of p-tau and NFTs in APP/PS1-TauP301L-Adeno AD mice

We investigated the progression of AD pathology in APP/PS1 mice when mutant tau overexpression and reactive astrogliosis were concurrently induced. To induce tau pathology, human mutant tau was overexpressed by injecting AAV_{DJ}-EF1α-hP301L-EGFP (AAV-TauP301L) into the DG and CA1 of the hippocampus of 5-month-old APP/PS1 mice. Immunostaining confirmed elevated levels of p-tau and NFTs upon AAV-TauP301L overexpression in both APP/PS1 mice and age-matched WT littermates. p-Tau levels were significantly increased in WT and APP/PS1 mice injected with AAV-TauP301L compared to mice injected with control virus (AAV_{DJ}-EF1α-EGFP) (Supplementary Figure S1A, B). The accumulation of p-tau was further increased when mutant tau was overexpressed in APP/PS1 mice (Figure 1A, C). In addition to p-tau, NFTs also significantly accumulated in AAV-TauP301L-injected APP/PS1 mice (Supplementary Figure S1A, C), indicating that Aβ synergistically mediates tau phosphorylation and NFT accumulation, in line with previous findings (Gomes et al., 2019). Furthermore, after induction of mutant tau in APP/PS1 mice, a concomitant increase in GFAP intensity was observed compared to APP/PS1 mice injected with the control virus (Figure 1A, B), suggesting that the accumulation of Aβ plaques and p-tau aggravates reactive astrogliosis.

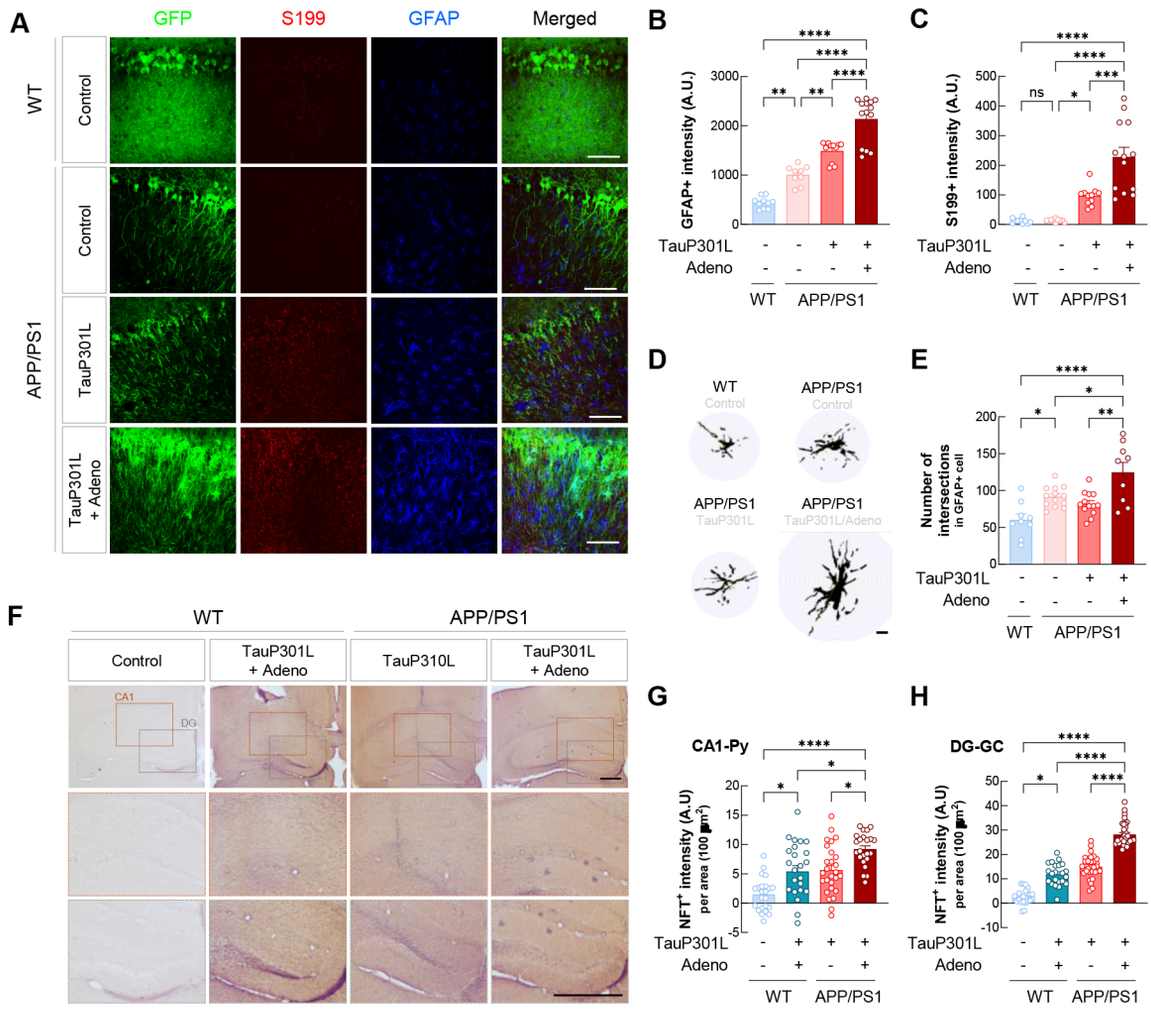

Figure 1 TauP301L overexpression and adenovirus-induced reactive astrogliosis in the hippocampus of APP/PS1 mice induces phosphorylated tau, reactive astrogliosis, and NFTs

A: Representative immunohistochemical images of S199 (p-tau, red) and GFAP (astrocyte, blue) in 8-month-old WT-Control, APP/PS1-Control, APP/PS1-TauP301L, and APP/PS1-TauP301L-Adeno mice. Scale bars: 40 μm. B, C: Bar graph showing mean intensity of GFAP (B) and S199 (C). Each bar represents mean±SEM. Sample sizes: WT-control (n=10), APP/PS1-Control (n=9), APP/PS1-TauP301L (n=11), APP/PS1-TauP301L-Adeno (n=14), n: number of slices, collected from 3–4 mice per group. Mean±SEM values: (B) WT-control=439.354±36.525, APP/PS1-Control=1 007.23±69.796, APP/PS1-TauP301L=1 489.587±61.307, APP/PS1-TauP301L-Adeno=2 137.64±123.507. (C) WT-control=11.963±2.66, APP/PS1-Control=13.645±1.712, APP/PS1-TauP301L=96.347±9.63, and APP/PS1-TauP301L-Adeno=227.446±32.95. D: Representative Sholl analysis images of GFAP-positive astrocytes in WT-Control, APP/PS1-Control, APP/PS1-TauP301L, and APP/PS1-TauP301L-Adeno mice. Circles centered around soma are separated by radial intervals of 10 μm. Scale bars: 50 μm. E: Bar graph showing number of intersections in GFAP-positive cells. Each bar represents mean±SEM. Sample sizes: WT-control (n=9), APP/PS1-Control (n=13), APP/PS1-TauP301L (n=13), APP/PS1-TauP301L-Adeno (n=9), n: GFAP-positive cells collected from 3–4 mice per group. Mean±SEM values: WT-control=60.333±7.878, APP/PS1-Control=91.538±3.847, APP/PS1-TauP301L=82.069±4.423, and APP/PS1-TauP301L-Adeno=124.666±13.497. F: Representative photomicrographs of NFTs stained using ABC/DAB in APP/PS1-TauP301L-Adeno brain sections. Scale bars: 500 μm. G, H: Bar graph showing quantification of NFT-positive intensity per area (100 μm^2) in CA1 and DG of hippocampus. Each bar represents mean±SEM. (G, CA1 pyramidal layer). Sample sizes: WT-Control (n=23), WT-TauP301L/Adeno (n=24), APP/PS1-TauP301L (n=27), and APP/PS1-TauP301L-Adeno (n=23). (H, DG granule cell layer) Sample sizes: WT-Control (n=22), WT-TauP301L/Adeno (n=22), APP/PS1-TauP301L (n=31), and APP/PS1-TauP301L-Adeno (n=33). Each dot represents an individual area measurement, with data collected from 3–6 mice per group. Mean±SEM values: (G, CA1 pyramidal layer) WT-Control=1.459±0.588, WT-TauP301L/Adeno=5.382±1.043, APP/PS1-TauP301L=5.647±0.804, APP/PS1-TauP301L-Adeno=9.199±0.576, (H, DG granule cell layer) WT-Control=2.604±0.662, WT-TauP301L/Adeno=11.88±0.964, APP/PS1-TauP301L=15.006±0.825, and APP/PS1-TauP301L-Adeno=28.19±0.832. Statistical analysis was conducted using one-way ANOVA with Tukey's *post-hoc* test, ns: Not significant; *: P<0.05; **: P<0.01; ***: P<0.001; ****: P<0.0001.

To further explore the impact of severe reactive astrogliosis, we co-injected Adeno-GFAP-GFP with AAV-TauP301L into the hippocampal DG and CA1 in APP/PS1 mice. Remarkably, this co-injection resulted in a marked enhancement of GFAP intensity compared to AAV-TauP301L injection alone (Figure 1A, B). In addition, astrocyte morphological changes, including increased branching and ramification, were significantly increased in APP/PS1-TauP301L-Adeno mice (Figure 1D, E). These findings indicate that Aβ plaques initiate astrocyte reactivity, which is subsequently enhanced by overexpression of AAV-TauP301L in APP/PS1 mice. Furthermore, the accumulation of Aβ plaques and p-tau, in

conjunction with adenovirus-induced reactive astrogliosis, profoundly intensifies the severity of astrocyte reactivity.

To investigate whether adenovirus-induced reactive astrogliosis with mutant tau overexpression exacerbates p-tau and NFT accumulation in APP/PS1 mice, p-tau and NFT immunostaining was performed after simultaneous injection of AAV-TauP301L and Adeno-GFAP-GFP into the hippocampal DG and CA1 regions of APP/PS1 mice. The accumulation of p-tau and NFTs notably increased when Adeno-GFAP-GFP was injected along with AAV-TauP301L in APP/PS1 mice (Figure 1A, C, F–H). These results suggest that severe reactive astrogliosis exacerbates tau pathology in the presence of mutant tau in APP/PS1 mice. Interestingly, NFT accumulation levels in WT mice co-injected with AAV-TauP301L and Adeno-GFAP-GFP were comparable to those observed in APP/PS1 mice injected with AAV-TauP301L alone, implying that Adeno-GFAP-GFP-induced reactive astrogliosis mimics the effects of Aβ plaque-induced reactive astrogliosis. Collectively, these findings suggest that interplay between Adeno-GFAP-GFP-induced severe reactive astrogliosis, AAV-TauP301L-induced p-tau expression, and Aβ pathology contributes to accelerated reactive gliosis and NFT accumulation in the hippocampus of APP/PS1 mice.

Overexpression of AAV-TauP301L and Adeno-GFAP-GFP enhances Aβ plaque accumulation in APP/PS1 mice

We next investigated the impact of mutant tau overexpression and adenovirus-induced reactive astrogliosis on Aβ plaque accumulation in APP/PS1 mice. Reactive astrocytes are known to exacerbate the pathological features of AD, contributing to glial activation, tauopathy, neuronal death, brain atrophy, cognitive impairment, and eventual death via H_2O_2 production (Chun et al., 2020). Based on these observations, we hypothesized that severe reactive astrocytes driven by Aβ plaques, mutant tau overexpression, and adenovirus-induced reactivity would further enhance Aβ plaque accumulation. Immunostaining for Aβ plaques in APP/PS1-TauP301L-Adeno mice exhibited significantly larger plaques in the hippocampus compared to controls (Figure 2A, B). This suggests that the combination of mutant tau overexpression and adenovirus-induced astrocyte reactivity amplifies reactive gliosis and NFT formation, subsequently accelerating Aβ plaque accumulation.

To further validate our hypothesis, thioflavin-S staining was used to assess Aβ deposition in the adjacent cortical regions. A progressive increase in Aβ deposition was observed in the somatosensory S1 cortex and piriform cortex of mice, with severity ranking as APP/PS1-Control, APP/PS1-TauP301L, and APP/PS1-TauP301L-Adeno, and WT mice (no deposition) (Figure 2C). The number of thioflavin-S-positive plaques in the somatosensory S1 cortex and piriform cortex of APP/PS1-TauP301L-Adeno mice significantly exceeded those in APP/PS1-Control and APP/PS1-TauP301L mice, indicating that adenovirus-induced reactive astrogliosis, coupled with mutant tau overexpression, accelerates Aβ accumulation (Figure 2D, E). APP/PS1-TauP301L mice also displayed significantly more Aβ plaques than APP/PS1-Control mice, supporting the notion that overexpression of mutant tau amplifies reactive astrogliosis (Figure 1A, B), further exacerbating Aβ plaque deposition. These findings imply that the induction of tau pathology and reactive astrogliosis is pivotal in accelerating Aβ deposition in APP/PS1-TauP301L-Adeno mice.

Abundant astrocytic GABA and increased MAO-B activity in APP/PS1-TauP301L-Adeno mice

Aberrant astrocytic GABA has been implicated in inhibiting neuronal activity and contributing to learning and memory impairments in AD (Jo et al., 2014). To evaluate astrocytic GABA levels in APP/PS1-TauP301L-Adeno mice, co-immunostaining of GABA and GFAP was performed on hippocampal slices. Astrocytes in APP/PS1-control mice exhibited a trend toward increased GABA immunoreactivity compared to age-matched WT mice. Furthermore, GFAP-positive astrocytes in APP/PS1-TauP301L and APP/PS1-TauP301L-Adeno mice displayed more robust GABA immunoreactivity compared to both APP/PS1-control and WT mice (Figure 3A, B).

MAO-B, a key enzyme involved in astrocytic GABA production, is up-regulated in post-mortem AD brain tissue and AD mouse models (Adolfsson et al., 1980; Jo et al., 2014). To assess the potential increase in MAO-B activity in the APP/PS1-TauP301L-Adeno AD mouse model, a fluorometric assay was performed on mitochondrial-rich fractions isolated from hippocampal tissue homogenates (Figure 3C). A substantial increase in MAO-B enzyme activity was observed in the hippocampus of APP/PS1 mice compared to WT mice (Figure 3D). Notably, MAO-B enzyme activity was significantly increased in APP/PS1-TauP301L and APP/PS1-TauP301L-Adeno mice compared to WT mice (Figure 3D). Treatment with selegiline, a selective and irreversible MAO-B inhibitor, significantly attenuated MAO-B activity across experimental groups (Figure 3D). These results suggest that mutant tau overexpression and adenovirus-induced reactive astrogliosis in the hippocampus of APP/PS1 mice can increase MAO-B activity, leading to the production and release of astrocytic GABA.

Acceleration of neuronal degeneration in the CA1 region of APP/PS1-TauP301L-Adeno mice

The formation of Aβ plaques and NFTs leads to neuronal loss (Knowles et al., 1999; Malek-Ahmadi et al., 2016). We hypothesized that neuronal loss would be exacerbated in APP/PS1 mice after the induction of mutant tau and adenovirus-induced reactive astrogliosis into the hippocampus. To test this, immunostaining with the neuronal marker NeuN was performed. Interestingly, a substantial reduction of NeuN signaling was observed in the CA1 pyramidal layer of APP/PS1-TauP301L-Adeno mice. In contrast, NeuN staining in age-matched WT, APP/PS1, and APP/PS1-TauP301L-Adeno mice remained intact (Figure 4A). Quantitative analysis confirmed a marked decrease in the number of NeuN-positive cells in the CA1 pyramidal layer of APP/PS1-TauP301L-Adeno mice (Figure 4B). These results indicate that neurodegeneration occurred within 3 months of AAV-TauP301L and Adeno-GFAP-GFP injections into the 5-month-old APP/PS1 mice. This finding suggests that APP/PS1-TauP301L-Adeno mice show an earlier onset of neuronal loss compared to the timeline reported in previous research, which identified neuronal loss in APP/PS1 mice at 17 months of age (Rupp et al., 2011).

Overexpression of P301L human mutant tau and severe reactive astrogliosis exacerbates hippocampus-dependent memory impairment in APP/PS1 mice

The impact of mutant tau overexpression and adenovirus-induced reactive astrogliosis on locomotor activity, anxiety, and hippocampus-dependent memory in APP/PS1 mice was

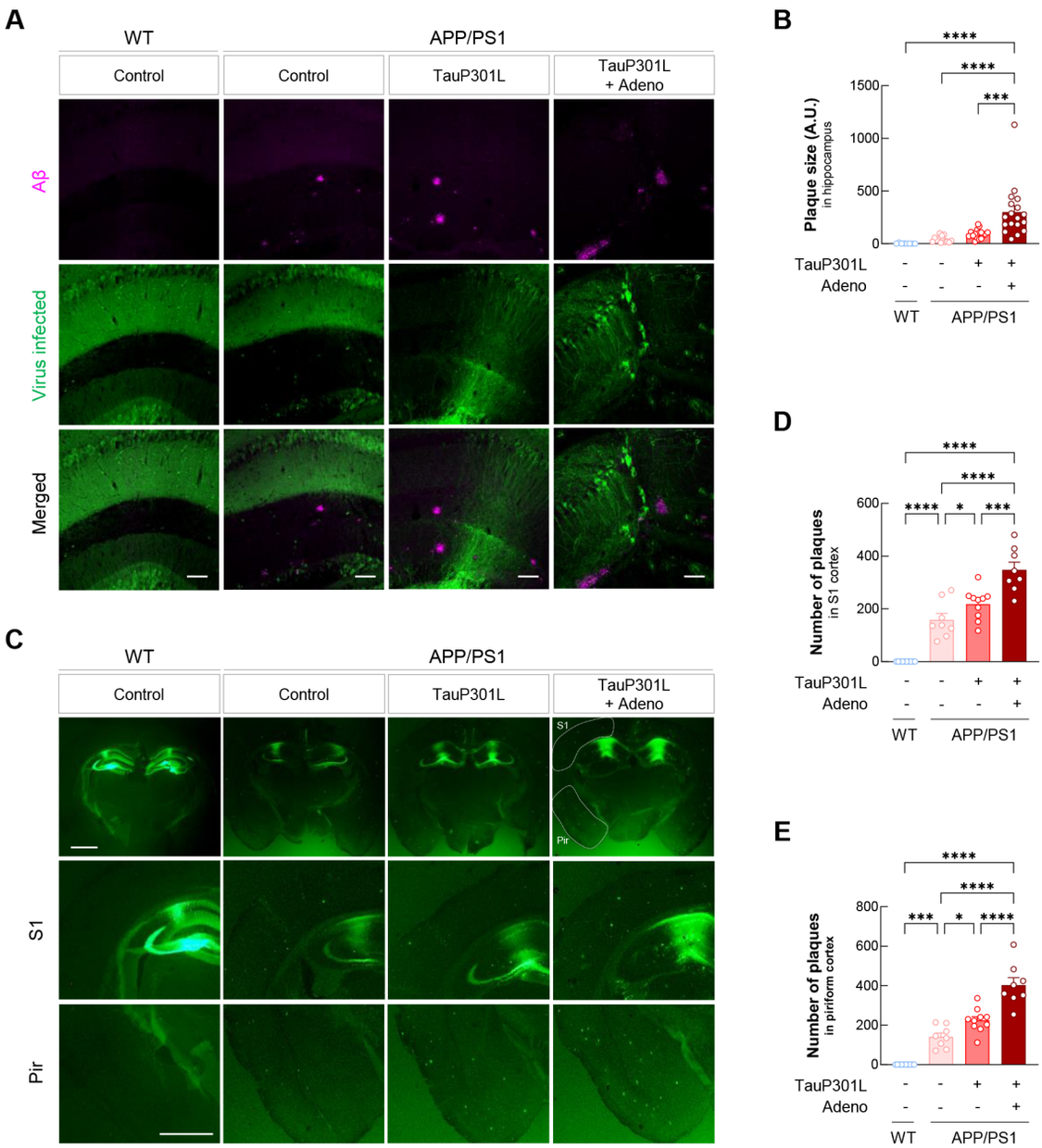

Figure 2 TauP301L overexpression and adenovirus-induced reactive astrogliosis in the hippocampus of APP/PS1 mice induces robust amyloid pathologies

A: Representative immunofluorescence images of Aβ (magenta) staining in hippocampal CA1 from WT-Control, APP/PS1-Control, APP/PS1-TauP301L, and APP/PS1-TauP301L-Adeno mice. Scale bars: 40 μm. B: Bar graph showing quantification of Aβ plaque size in the hippocampus. Each bar represents mean±SEM. Sample sizes: WT-control (*n*=8), APP/PS1-Control (*n*=13), APP/PS1-TauP301L (*n*=17), APP/PS1-TauP301L-Adeno (*n*=18), *n*: number of slices, collected from three mice per group. Mean±SEM values: WT-control=1.924±1.329, APP/PS1-Control=40.663±8.291, APP/PS1-TauP301L=91.938±10.201, and APP/PS1-TauP301L-Adeno=299.923±57.433. C: Representative images showing Aβ plaques stained with thioflavin-S (thio-S). S1 indicates S1 somatosensory cortex, Pir indicates piriform cortex. Scale bars: 1 mm. D, E: Bar graph showing quantification of number of Aβ plaques in the S1 somatosensory cortex (D) and piriform cortex (E). Each bar represents mean±SEM. Sample sizes: (D, E) WT-control (*n*=10), APP/PS1-Control (*n*=8), APP/PS1-TauP301L (*n*=10), APP/PS1-TauP301L-Adeno (*n*=8), with data collected from three mice per group. Mean±SEM values: (D) WT-control=0, APP/PS1-Control=158.038±24.752, APP/PS1-TauP301L=217.972±18.255, APP/PS1-TauP301L-Adeno=347.858±29.539. (E) WT-control=0, APP/PS1-Control=140.775±19.422, APP/PS1-TauP301L=224.287±18.873, APP/PS1-TauP301L-Adeno=402.746±37.664. Statistical analysis was conducted using one-way ANOVA with Tukey's *post-hoc* test, *: P<0.05; ***: P<0.001; ****: P<0.0001.

systematically evaluated. Locomotor activity and anxiety levels were assessed using the open field test (Supplementary Figure S2A). Total distance traveled revealed increased locomotor activity in both APP/PS1-TauP301L and APP/PS1-TauP301L-Adeno mice, consistent with previous findings (Jul et al., 2016; Wang et al., 2022) (Supplementary Figure S2B). However, neither the distance traveled nor time spent in the center zone differed significantly between groups, suggesting that anxiety levels were unaltered by mutant tau overexpression or additional reactive astrogliosis induction (Supplementary Figure S2C, D).

Hippocampus-dependent memory and cognitive

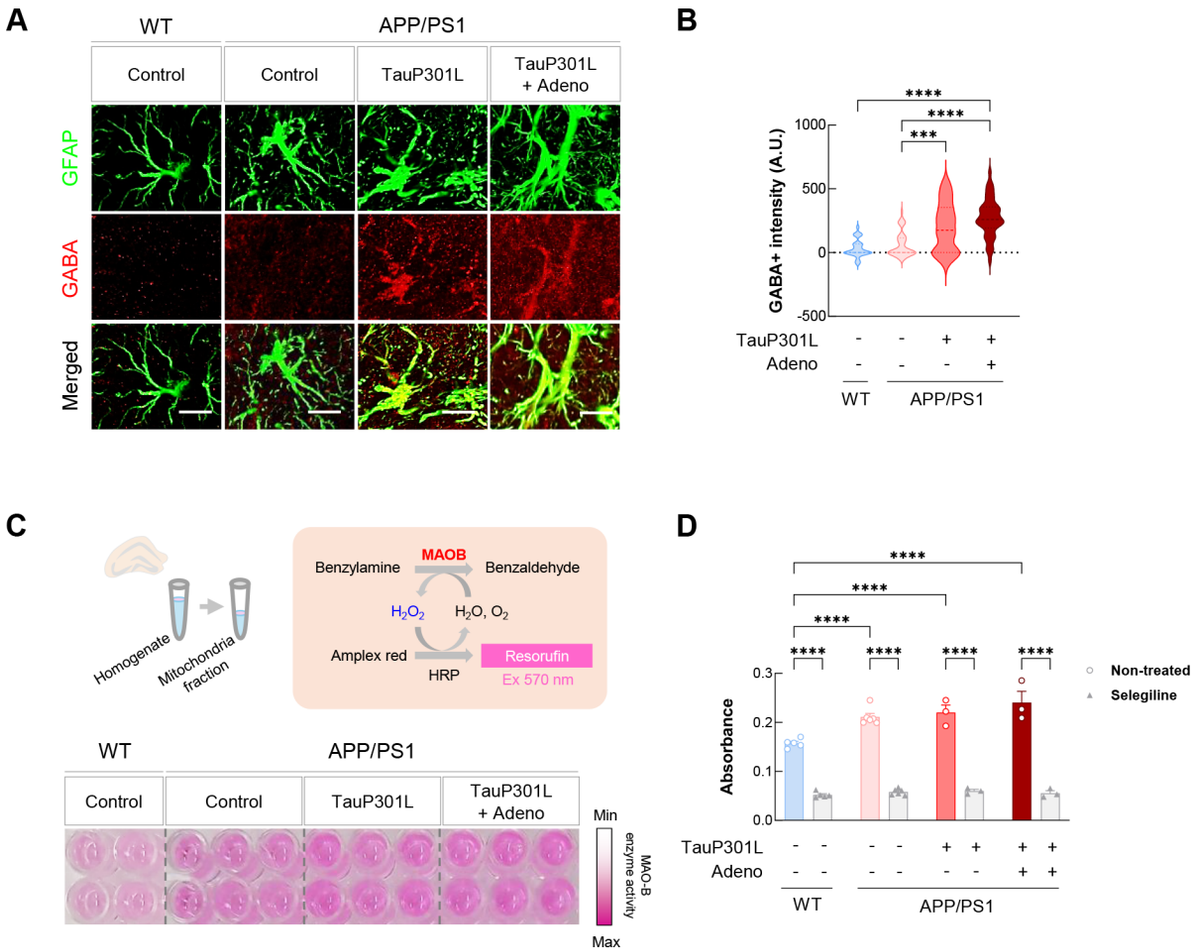

Figure 3 TauP301L overexpression and adenovirus-induced reactive astrogliosis in the hippocampus of APP/PS1 mice increases astrocytic GABA and MAO-B enzyme activity

A: Representative confocal images of astrocytes (GFAP, green) and GABA (red) in the molecular layer of CA3 from 8-month-old WT-Control, APP/PS1-Control, APP/PS1-TauP301L, and APP/PS1-TauP301L-Adeno mice. Scale bars: 5 μm. B: Violin plots showing GABA intensity in GFAP-positive astrocytes, representing the distribution of data within each group. Dashed lines indicate median, dotted lines represent quartiles. Sample sizes: WT-Control (*n*=28), APP/PS1-Control (*n*=38), APP/PS1-TauP301L (*n*=31), APP/PS1-TauP301L/Adeno (*n*=41), with GFAP-positive cells collected from four mice per group. Mean±SEM values: WT-Control=31.931±13.091, APP/PS1-Control=61.623±15.829, APP/PS1-TauP301L=200.939±33.855, and APP/PS1-TauP301L-Adeno=274.775±23.761. C: Schematic of MAO-B enzyme activity assay in the hippocampus (Top). Representative images of color change after 20 min of MAO-B reaction (Bottom, *n*=2 for 8-month-old WT-Control; *n*=3 for other groups). D: Bar graph showing MAO-B enzyme activity measured by absorbance at 570 nm in hippocampal tissue. Each bar represents mean absorbance±SEM, with sample sizes: WT-Control (*n*=5), APP/PS1-Control (*n*=6), APP/PS1-TauP301L (*n*=3), and APP/PS1-TauP301L-Adeno (*n*=3). One hippocampal tissue sample from one hemisphere was examined per mouse. Mean absorbance±SEM values: non-treated WT-control=0.157±0.004, selegiline-treated WT-control=0.052±0.003; non-treated APP/PS1-Control=0.211±0.007, selegiline-treated APP/PS1-Control=0.058±0.003; on-treated APP/PS1-TauP301L=0.22±0.015, selegiline-treated APP/PS1-TauP301L=0.06±0.004; non-treated APP/PS1-TauP301L-Adeno=0.24±0.023, and selegiline-treated APP/PS1-TauP301L-Adeno=0.24±0.023. Statistical analysis was conducted using one-way ANOVA with Tukey's *post-hoc* test, ***: *P*<0.001; ****: *P*<0.0001.

impairments in 8-month-old APP/PS1-TauP301L-Adeno mice were further investigated using the NOR task, Y-maze test, and passive avoidance test (Figure 5A, D, G). During the NOR familiarization phase, all groups exhibited no preference for any specific object. In the testing session, WT, APP/PS1, WT-TauP301L/Adeno, and APP/PS1-TauP301L mice demonstrated a preference for the novel object, while APP/PS1-TauP301L-Adeno mice failed to exhibit this preference, indicating impaired recognition memory (Figure 5B, C).

Spatial working memory was assessed using the Y-maze test, which records sequences of arm entries to analyze the percentage of spontaneous alternations (Figure 5D). APP/PS1-TauP301L-Adeno mice exhibited a significant reduction in spontaneous alternations compared to age-matched WT and APP/PS1-TauP301L mice, highlighting deficits in spatial working memory (Figure 5E, F). These results suggest that adenovirus-induced reactive astrogliosis, together with mutant tau overexpression, not only accelerates pathological features of AD, such as NFT and Aβ plaque accumulation, severe reactive astrocytes, neuronal loss, and elevation of astrocytic GABA levels, but also contributes to hippocampus-dependent memory impairment.

To further corroborate these findings, cognitive dysfunction and memory performance were evaluated using the passive avoidance test (Figure 5G). During the acquisition phase, no significant differences were observed in the time taken to enter the dark chamber across groups, indicating similar

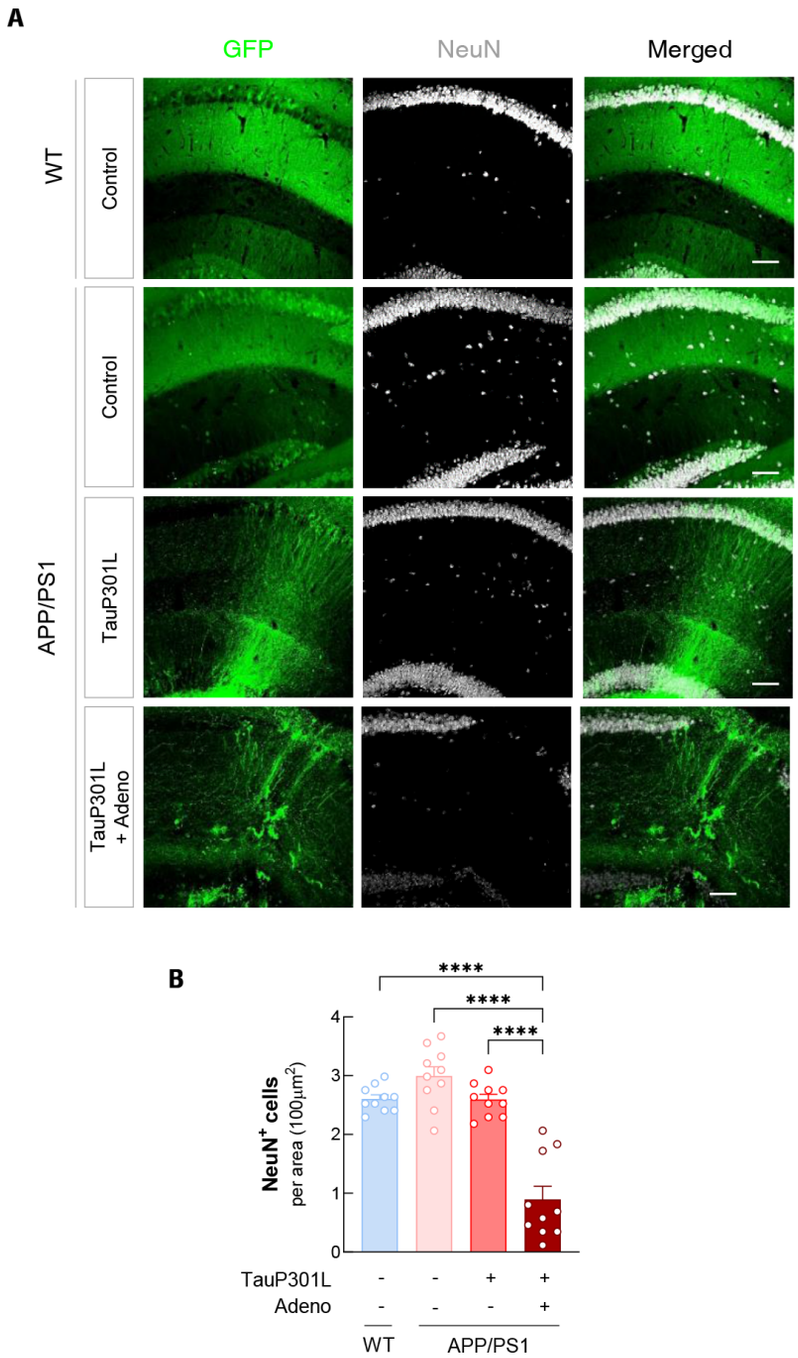

Figure 4 TauP301L overexpression and adenovirus-induced reactive astrogliosis in the hippocampus of APP/PS1 mice accelerates neurodegeneration

A: Representative confocal images of NeuN (neuron, white) in the CA1 pyramidal layer of 8-month-old WT-Control, APP/PS1-Control, APP/PS1-TauP301L, and APP/PS1-TauP301L-Adeno mice. Scale bars: 40 μm. B: Bar graph showing number of NeuN-positive cells per area (100 μm^2). Each bar represents mean±SEM. Sample sizes for all groups: n=10, with each dot representing the average count from three area per slice. Ten slices were analyzed from 3–4 mice per group. Mean±SEM values: WT-Control=2.605±0.069, APP/PS1-Control=2.995±0.157, APP/PS1-TauP301L=2.593±0.091, and APP/PS1-TauP301L-Adeno=0.895±0.226). Statistical analysis was conducted using one-way ANOVA with Tukey's *post-hoc* test, ****: P<0.0001.

baseline anxiety levels. During the retention phase conducted 24 h post-electrical shock, the APP/PS1-TauP301L-Adeno mice displayed a significantly shorter latency to enter the dark chamber compared to WT mice (Figure 5H), indicating that the simultaneous induction of mutant tau and adenovirus-induced reactive astrogliosis in APP/PS1 mice exacerbates impairment of hippocampus-dependent memory, consistent with the NOR and Y-maze results.

Taken together, these findings establish APP/PS1-TauP301L-Adeno mice as a robust animal model of AD, in which augmented reactive astrogliosis by Adeno-GFAP-GFP infection in the presence of toxic molecules such as Aβ and p-Tau further amplifies the aggregation of Aβ plaques and NFTs, ultimately exacerbating pathological symptoms of AD, such as neuronal loss and memory deficits (Figure 6). This model offers a valuable tool for investigating the mechanistic

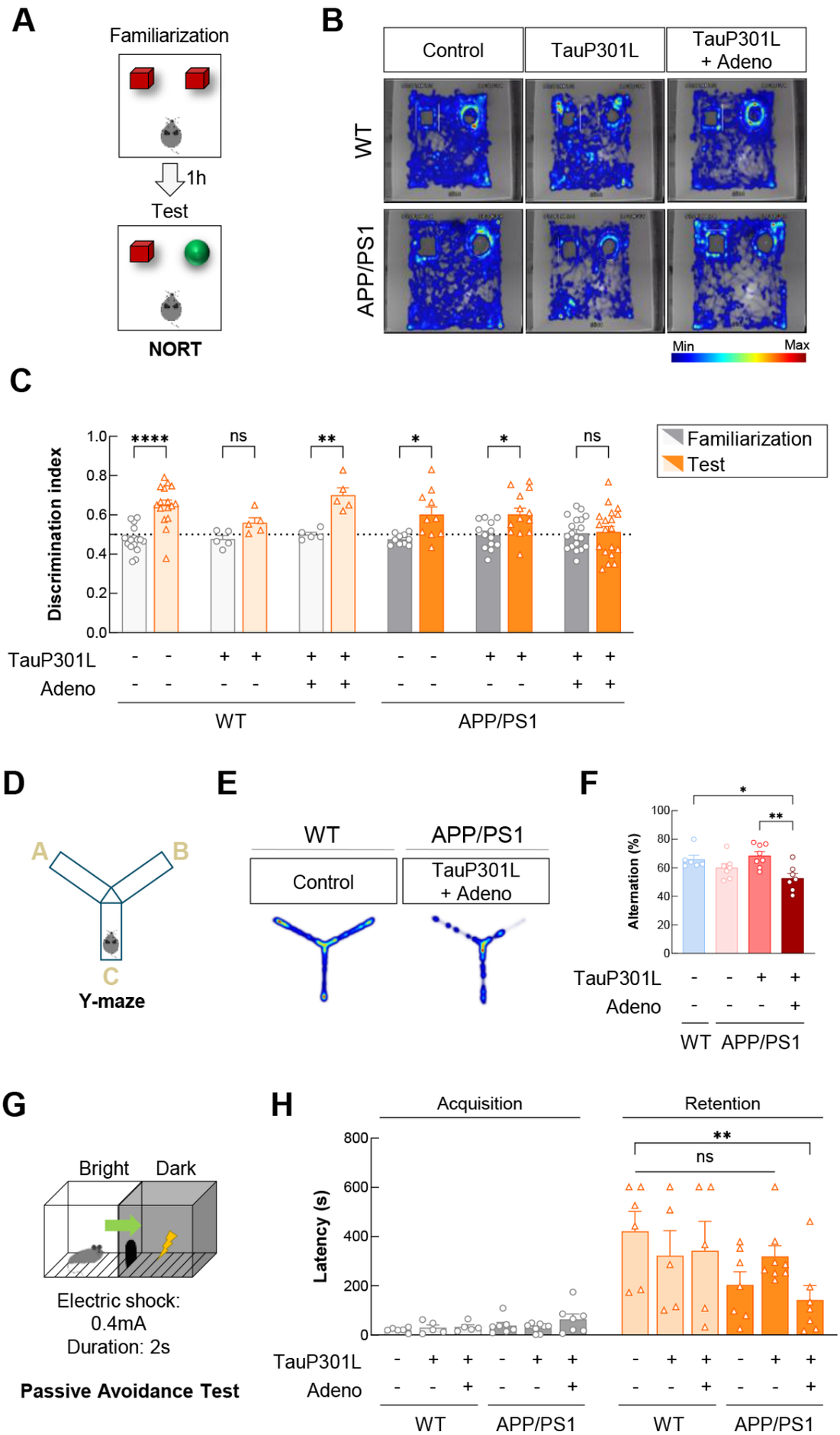
A
Familiarization
1h
Test
NORT
B
Control
TauP301L
TauP301L + Adeno
WT
APP/PS1
Min
Max
C
Discrimination index
1.0
0.8
0.6
0.4
0.2
0.0
****
ns
**
*
*
ns
Familiarization
Test
TauP301L
Adeno
WT
APP/PS1
D
A
B
C
Y-maze
E
WT
APP/PS1
Control
TauP301L + Adeno
F
Alternation (%)
100
80
60
40
20
0
*
**
TauP301L
Adeno
WT
APP/PS1
G
Bright
Dark
Electric shock:
0.4mA
Duration: 2s
Passive Avoidance Test
H
Acquisition
Retention
Latency (s)
800
600
400
200
0
**
ns
TauP301L
Adeno
WT
APP/PS1
WT
APP/PS1

Figure 5 TauP301L overexpression and adenovirus-induced reactive astrogliosis in the hippocampus of APP/PS1 mice impairs hippocampus-dependent memory

A, B: Schematic of novel object recognition (NOR) test (A) and representative heatmap image in NOR square chamber (gray) during test session (B). C: Bar graph showing discrimination index, calculated as: Discrimination index=exploration time in novel object/total exploration time (novel+familiar). Each bar represents mean±SEM, with sample sizes (number of mice): WT-Control (n=16), WT-TauP301L (n=5), WT-TauP301L/Adeno (n=5), APP/PS1-Control (n=10), APP/PS1-TauP301L (n=13), and APP/PS1-TauP301L-Adeno (n=19). Statistical analysis was conducted using two-way ANOVA with Bonferroni test, ns: Not significant; *: P<0.05; **: P<0.01; ****: P<0.0001. Mean±SEM values: (Familiarization) WT-Control=0.475±0.016, WT-TauP301L=0.475±0.019, WT-TauP301L/Adeno=0.499±0.012, APP/PS1-Control=0.476±0.009, APP/PS1-TauP301L=0.497±0.019 and APP/PS1-TauP301L-Adeno=0.507±0.019. (Test) WT-Control=0.65±0.026, WT-TauP301L=0.56±0.025, WT-TauP301L/Adeno=0.7±0.037, APP/PS1-Control=0.602±0.039, APP/PS1-TauP301L=0.603±0.031, and APP/PS1-TauP301L-Adeno=0.513±0.028. D, E: Schematic of Y-maze (D) and representative heatmap of tracks (E) in Y-maze spontaneous alternation test. F: Bar graph showing average percentage of triad alternations relative to total arm entries. Each bar represents mean±SEM, with sample sizes (number of mice): WT-Control (n=6), APP/PS1-Control (n=7), APP/PS1-TauP301L (n=8), and APP/PS1-TauP301L-Adeno (n=7). Statistical analysis was conducted using one-way ANOVA with Tukey's *post-hoc* test, *: P<0.05; **: P<0.01. Mean±SEM values: WT-Control=65.855±2.892, APP/PS1-Control=59.946±2.999, APP/PS1-TauP301L=68.399±2.794, and APP/PS1-TauP301L-Adeno=52.629±3.402. G: Schematic of passive avoidance test (PAT). H: Bar graph showing time for latency to enter dark chamber. Each bar represents mean±SEM, with sample sizes (number of mice): WT-Control (n=6), WT-TauP301L (n=5), WT-TauP301L-Adeno (n=5), APP/PS1-Control (n=7), APP/PS1-TauP301L (n=8), and APP/PS1-TauP301L-Adeno (n=7). Statistical analysis was conducted using two-way ANOVA with Bonferroni test, ns: Not significant; **: P<0.01. Mean±SEM values: (Acquisition) WT-Control=20.75±3.748, WT-TauP301L=29.8±10.918, WT-TauP301L-Adeno=32.9±8.532, APP/PS1-Control=38.214±12.636, APP/PS1-TauP301L=29.188±6.408, APP/PS1-TauP301L-Adeno=63.886±21.87. (Retention) WT-Control=421.85±80.612, WT-TauP301L=322.5±101.528, WT-TauP301L-Adeno=342.4±119.582, APP/PS1-Control=203.614±53.403, APP/PS1-TauP301L=319.55±43.637, and APP/PS1-TauP301L-Adeno=142.471±58.3.

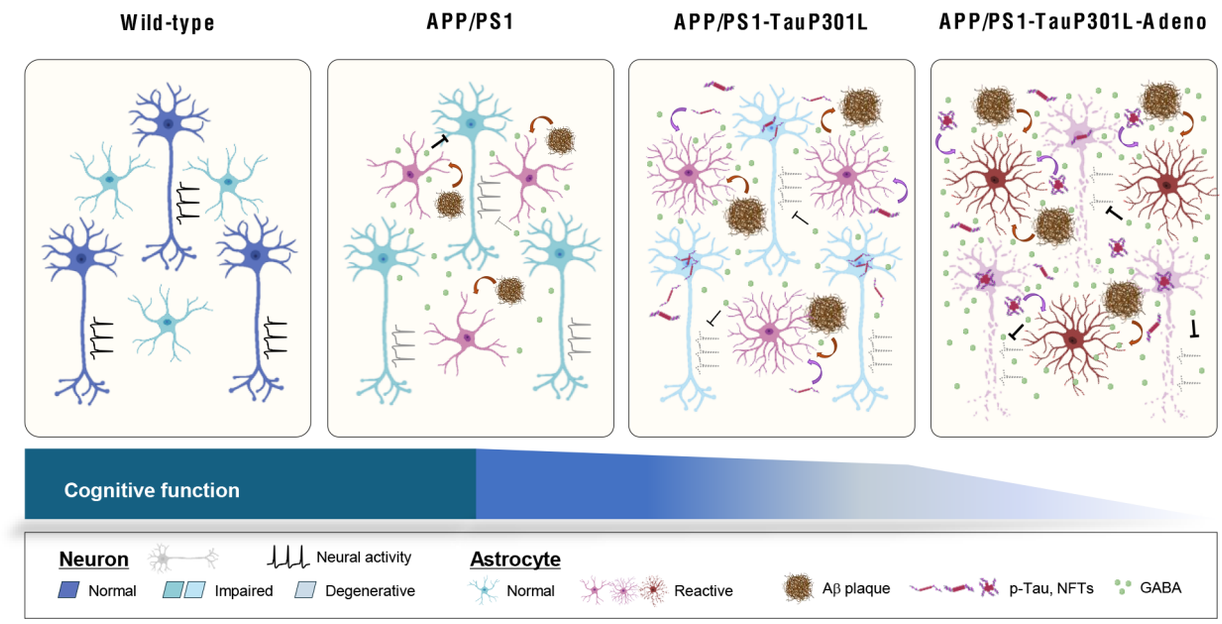

Figure 6 Summary of APP/PS1-TauP301L-Adeno mouse model

Summary figure illustrates progression of pathological features in both APP/PS1-TauP301L and APP/PS1-TauP301L-Adeno mice. At 8 months of age, 3 months post-injection, APP/PS1-TauP301L mice exhibited increased reactive astrogliosis and accumulation of Aβ plaque in the hippocampus compared to APP/PS1-control mice, but did not display any significant impairment of hippocampus-dependent cognitive function. In contrast, APP/PS1-TauP301L-Adeno mice showed exacerbated reactive astrogliosis and further accumulation of Aβ plaques, as well as NFT development, further exacerbating hippocampus-dependent cognitive impairment.

interplay between reactive astrogliosis, tau pathology, and Aβ deposition in AD progression.

DISCUSSION

As a highly prevalent neurodegenerative disorder, AD is characterized by cognitive decline, neuronal loss, and hippocampal atrophy, with key pathological features such as Aβ plaques, p-tau, and NFTs. Inflammatory responses, such as microglial activation and reactive astrogliosis, are also integral components of AD pathology (Bloom, 2014; Kinney et al., 2018). Current treatment options provide limited symptomatic relief and fail to modify the underlying disease progression, highlighting the need for a deeper understanding of disease mechanisms and the development of early-stage therapeutic strategies before irreversible pathological changes occur.

Reliable animal models that accurately recapitulate AD pathophysiology are critical for advancing preventive, diagnostic, and therapeutic approaches. Among these, APP/PS1 mice, which harbor familial AD-associated mutations in the *APP* and *PS1* genes, are widely used in AD research (Chen & Zhang, 2022; Wang et al., 2024). This model exhibits hallmark features of AD, including reactive astrocytes and

activated microglia surrounding Aβ deposits as early as 2 months of age (Radde et al., 2006) and mild memory impairment from 5 months of age (Zhu et al., 2017). Astrocytes are known to respond to Aβ, with reactive astrogliosis histologically detectable before plaque formation (Heneka et al., 2005; Pike et al., 1994), suggesting that reactive astrogliosis may serve as an early indicator of neurological disorders.

Several studies have demonstrated that aberrant tonic GABA released from reactive astrocytes activates extrasynaptic $GABA_A$ receptors on neighboring neurons, leading to impaired neuronal activity and memory deficits (Chun et al., 2020; Jo et al., 2014). These findings highlight a pivotal role for reactive astrogliosis in early AD pathology, with synaptic dysfunction occurring before overt neurodegeneration. Notably, neuronal death is not observed in APP/PS1 mice until approximately 12 months of age (Matousek et al., 2012), with modest neuronal loss becoming apparent only by 17 months (Rupp et al., 2011). These observations suggest that memory deficits in AD are initially driven by synaptic impairments mediated by reactive astrogliosis, rather than by direct neuronal loss.

The 6xTg mouse model, generated by crossbreeding 5xFAD mice with TauP301L-expressing mice, has recently been introduced as a potential model for AD. This model exhibits rapid onset of pathology, with Aβ deposits appearing at 2 months of age, NFTs developing by 4 months of age, and cognitive impairment detectable as early as 2 months of age (Kang et al., 2021). Despite the rapid onset of histological pathology and cognitive decline in 6xTg mice, establishing causal relationships among amyloid pathology, tau pathology, and reactive astrogliosis remains challenging.

To address these limitations, we developed the APP/PS1-TauP301L-Adeno mouse model, designed to investigate the individual effects of Aβ plaques, mutant tau, and reactive astrogliosis on AD progression in a spatially and temporally specific manner (Figure 6). This optimized model demonstrated intensified Aβ deposition (Figure 2), increased NFT formation (Figure 1), and severe reactive astrogliosis (Figure 1) at 8 months of age, 3 months after the introduction of both mutant tau overexpression and adenovirus-induced reactive astrogliosis into the hippocampus of APP/PS1 mice. These pathological changes were associated with accelerated neuronal loss (Figure 4) and significant memory deficits (Figure 5).

In contrast, APP/PS1 mice with mutant tau overexpression alone, without adenovirus-induced reactive astrogliosis, exhibited only minor pathological changes. Although slight but significant increases in astrogliosis, p-tau, and Aβ plaque accumulation were observed compared to APP/PS1-Control mice, these mice showed no substantial neurodegeneration or memory impairment (Figures 4, 5). These results highlight the critical role of adenovirus-induced reactive astrogliosis in exacerbating the neurodegenerative and cognitive deficits associated with Aβ plaques and p-tau. In addition to the various pathological phenotypes and symptoms identified in our novel animal model, further research is needed to validate additional pathological features of AD, such as synapse loss and microglial activation.

Interestingly, reactive astrocytes play a paradoxical role in neurodegenerative diseases. On the one hand, astrocytes initiate detoxification pathways, such as the autophagy-to-urea pathway, to clear toxic molecules including Aβ oligomers and diphtheria toxin (Chun et al., 2020; Ju et al., 2022; Kim et al., 2024). However, in AD mouse models, Aβ accumulation disrupts astrocytic autophagy, which exacerbates Aβ plaque accumulation (Kim et al., 2024). The addition of tau pathology in APP/PS1 mice, such as NFT formation, may further disrupt astrocytic autophagy, thereby accelerating Aβ plaque accumulation (Figure 2). Although the autophagy-to-urea cycle is generally beneficial, its downstream product, putrescine, is metabolized into GABA via the MAO-B activity, a process with detrimental implications (Ju et al., 2022). Astrocytic GABA impairs CA1 pyramidal neuronal activity and contributes to memory deficits in APP/PS1 mice (Jo et al., 2014; Park et al., 2019). In addition to GABA production, severe astrocytic reactivity leads to neurodegeneration and brain atrophy through MAO-B and its by-product, H_2O_2 (Chun et al., 2020). Given these findings, future studies are needed to investigate the involvement of H_2O_2 in neurodegeneration and memory deficits in APP/PS1-TauP301L-Adeno mice.

Our animal model, in line with previous studies, primarily focuses on early-onset familial AD associated with mutations in APP, PS1, and TauP301L (Chen & Zhang, 2022; Wang et al., 2024). However, the majority of AD cases involve late-onset sporadic AD, which is not linked to specific genetic mutations. The absence of a clear genetic marker for sporadic AD presents a significant challenge in developing appropriate animal models (Chen & Zhang, 2022). Emerging evidence suggests that mitochondrial dysfunction, oxidative stress, and neuroinflammation in reactive astrocytes (Chun et al., 2020; Ju et al., 2022; Kim et al., 2024) may precede the abundant accumulation of Aβ plaques or Tau pathology (Krstic & Knuesel, 2013; Zlokovic, 2011). These early disruptions may play a critical role in the pathogenesis of late-onset sporadic AD. Thus, we propose that reactive astrocytes induced by Adeno-GFAP-GFP may also serve as a valuable strategy for sporadic AD research.

In conclusion, this study introduces APP/PS1-TauP301L-Adeno mice as a promising and novel AD mouse model. By leveraging spatial and temporal-specific genetic manipulation of tau pathology and reactive astrogliosis through the injection of AAV-TauP301L and Adeno-GFAP-GFP into the hippocampus of APP/PS1 mice, this model recapitulates key pathological hallmarks of AD. Notably, these mice exhibit a marked increase in Aβ plaques and tau pathology, manifesting significantly earlier than in established APP/PS1 mice. This time-efficient model provides a promising framework for studying AD progression and exploring therapeutic interventions, with potential applicability to both familial and sporadic forms of the disease.

SUPPLEMENTARY DATA

Supplementary data to this article can be found online.

COMPETING INTERESTS

The authors declare that they have no competing interests.

AUTHORS' CONTRIBUTIONS

S.J.O. and M.H.N. conceived and designed the project. Y.E.H. and S.L. performed the behavioral and molecular experiments, immunohistochemical analysis, and statistical analyses, and wrote the manuscript. S.E.L. designed the viral vector and produced all types of virus we used. M.H.N. provided technical support and conceptual advice. S.J.O. supervised the project. All authors read and approved the final version of the manuscript.

REFERENCES

Adolfsson R, Gottfries CG, Oreland L, et al. 1980. Increased activity of brain and platelet monoamine oxidase in dementia of Alzheimer type. *Life Sciences*, **27**(12): 1029–1034.

An H, Lee H, Yang S, et al. 2021. Adenovirus-induced reactive astrogliosis exacerbates the pathology of Parkinson's disease. *Experimental Neurobiology*, **30**(3): 222–231.

Bardehle S, Krüger M, Buggenthin F, et al. 2013. Live imaging of astrocyte responses to acute injury reveals selective juxtavascular proliferation. *Nature Neuroscience*, **16**(5): 580–586.

Bloom GS. 2014. Amyloid-β and Tau: the trigger and bullet in Alzheimer disease pathogenesis. *JAMA Neurology*, **71**(4): 505–508.

Chen ZY, Zhang Y. 2022. Animal models of Alzheimer's disease: applications, evaluation, and perspectives. *Zoological Research*, **43**(6): 1026–1040.

Chun H, Im H, Kang YJ, et al. 2020. Severe reactive astrocytes precipitate pathological hallmarks of Alzheimer's disease via $H_2O_2^-$ production. *Nature Neuroscience*, **23**(12): 1555–1566.

Di J, Cohen LS, Corbo CP, et al. 2016. Abnormal tau induces cognitive impairment through two different mechanisms: synaptic dysfunction and neuronal loss. *Scientific Reports*, **6**: 20833.

Drummond E, Wisniewski T. 2017. Alzheimer's disease: experimental models and reality. *Acta Neuropathologica*, **133**(2): 155–175.

Gomes LA, Hipp SA, Rijal Upadhaya A, et al. 2019. Aβ-induced acceleration of Alzheimer-related τ-pathology spreading and its association with prion protein. *Acta Neuropathologica*, **138**(6): 913–941.

Heneka MT, Sastre M, Dumitrescu-Ozimek L, et al. 2005. Focal glial activation coincides with increased BACE1 activation and precedes amyloid plaque deposition in APP[V717I] transgenic mice. *Journal of Neuroinflammation*, **2**: 22.

Ingelsson M, Fukumoto H, Newell KL, et al. 2004. Early Aβaccumulation and progressive synaptic loss, gliosis, and tangle formation in AD brain. *Neurology*, **62**(6): 925–931.

Jackson RJ, Rudinskiy N, Herrmann AG, et al. 2016. Human tau increases amyloid βplaque size but not amyloid β-mediated synapse loss in a novel mouse model of Alzheimer's disease. *European Journal of Neuroscience*, **44**(12): 3056–3066.

Jiwaji Z, Tiwari SS, Avilés-Reyes RX, et al. 2022. Reactive astrocytes acquire neuroprotective as well as deleterious signatures in response to Tau and Ass pathology. *Nature Communications*, **13**(1): 135.

Jo S, Yarishkin O, Hwang YJ, et al. 2014. GABA from reactive astrocytes impairs memory in mouse models of Alzheimer's disease. *Nature Medicine*, **20**(8): 886–896.

Ju YH, Bhalla M, Hyeon SJ, et al. 2022. Astrocytic urea cycle detoxifies Aβ-derived ammonia while impairing memory in Alzheimer's disease. *Cell Metabolism*, **34**(8): 1104–1120. e8.

Jul P, Volbracht C, de Jong IEM, et al. 2016. Hyperactivity with agitative-like behavior in a mouse tauopathy model. *Journal of Alzheimer's Disease*, **49**(3): 783–795.

Kang S, Kim J, Chang KA. 2021. Spatial memory deficiency early in 6xTg Alzheimer's disease mouse model. *Scientific Reports*, **11**(1): 1334.

Kato S, Gondo T, Hoshii Y, et al. 1998. Confocal observation of senile plaques in Alzheimer's disease: senile plaque morphology and relationship between senile plaques and astrocytes. *Pathology International*, **48**(5): 332–340.

Kim S, Chun H, Kim Y, et al. 2024. Astrocytic autophagy plasticity modulates Aβ clearance and cognitive function in Alzheimer's disease. *Molecular Neurodegeneration*, **19**(1): 55.

Kinney JW, Bemiller SM, Murtishaw AS, et al. 2018. Inflammation as a central mechanism in Alzheimer's disease. *Alzheimer's & Dementia*: *Translational Research & Clinical Interventions*, **4**: 575–590.

Knowles RB, Wyart C, Buldyrev SV, et al. 1999. Plaque-induced neurite abnormalities: implications for disruption of neural networks in Alzheimer's disease. *Proceedings of the National Academy of Sciences of the United States of America*, **96**(9): 5274–5279.

Krstic D, Knuesel I. 2013. Deciphering the mechanism underlying late-onset Alzheimer disease. *Nature Reviews Neurology*, **9**(1): 25–34.

Lee Y, Messing A, Su M, et al. 2008. *GFAP* promoter elements required for region-specific and astrocyte-specific expression. *Glia*, **56**(5): 481–493.

Malek-Ahmadi M, Perez SE, Chen KW, et al. 2016. Neuritic and diffuse plaque associations with memory in non-cognitively impaired elderly. *Journal of Alzheimer's Disease*, **53**(4): 1641–1652.

Matousek SB, Ghosh S, Shaftel SS, et al. 2012. Chronic IL-1β-mediated neuroinflammation mitigates amyloid pathology in a mouse model of Alzheimer's disease without inducing overt neurodegeneration. *Journal of Neuroimmune Pharmacology*, **7**(1): 156–164.

Nam MH, Cho J, Kwon DH, et al. 2020. Excessive astrocytic GABA causes cortical hypometabolism and impedes functional recovery after subcortical stroke. *Cell Reports*, **32**(3): 107975.

Nam MH, Ko HY, Kim D, et al. 2023. Visualizing reactive astrocyte-neuron interaction in Alzheimer's disease using ^{11}C-acetate and ^{18}F-FDG. *Brain*, **146**(7): 2957–2974.

Park JH, Ju YH, Choi JW, et al. 2019. Newly developed reversible MAO-B inhibitor circumvents the shortcomings of irreversible inhibitors in Alzheimer's disease. *Science Advances*, **5**(3): eaav0316.

Pike CJ, Cummings BJ, Monzavi R, et al. 1994. β-amyloid-induced changes in cultured astrocytes parallel reactive astrocytosis associated with senile plaques in Alzheimer's disease. *Neuroscience*, **63**(2): 517–531.

Querfurth HW, Laferla FM. 2010. Alzheimer's disease. *New England Journal of Medicine*, **362**(4): 329–344.

Radde R, Bolmont T, Kaeser SA, et al. 2006. Aβ42-driven cerebral amyloidosis in transgenic mice reveals early and robust pathology. *EMBO Reports*, **7**(9): 940–946.

Rupp NJ, Wegenast-Braun BM, Radde R, et al. 2011. Early onset amyloid lesions lead to severe neuritic abnormalities and local, but not global neuron loss in APPPS1 transgenic mice. *Neurobiology of Aging*, **32**(12): 2324.e1–6.

Selkoe D, Kopan R. 2003. Notch and presenilin: regulated intramembrane proteolysis links development and degeneration. *Annual Review of Neuroscience*, **26**: 565–597.

Shirley JL, De Jong YP, Terhorst C, et al. 2020. Immune responses to viral gene therapy vectors. *Molecular Therapy*, **28**(3): 709–722.

Simpson JE, Ince PG, Lace G, et al. 2010. Astrocyte phenotype in relation to Alzheimer-type pathology in the ageing brain. *Neurobiology of Aging*, **31**(4): 578–590.

Wang Q, Zhu BT, Lei P. 2024. Animal models of Alzheimer's disease: Current strategies and new directions. *Zoological Research*, **45**(6): 1385–1407.

Wang TQ, Chen Y, Zou Y, et al. 2022. Locomotor hyperactivity in the early-stage Alzheimer's disease-like pathology of APP/PS1 mice: associated with impaired polarization of astrocyte aquaporin 4. *Aging and Disease*, **13**(5): 1504–1522.

Woo J, Im SK, Chun H, et al. 2017. Functional characterization of resting and adenovirus-induced reactive astrocytes in three-dimensional culture. *Experimental Neurobiology*, **26**(3): 158–167.

Yamada T, Kawamata T, Walker DG, et al. 1992. Vimentin immunoreactivity in normal and pathological human brain tissue. *Acta Neuropathologica*, **84**(2): 157–162.

Zhu SH, Wang JH, Zhang YB, et al. 2017. The role of neuroinflammation and amyloid in cognitive impairment in an APP/PS1 transgenic mouse model of Alzheimer's disease. *CNS Neuroscience & Therapeutics*, **23**(4): 310–320.

Zlokovic BV. 2011. Neurovascular pathways to neurodegeneration in Alzheimer's disease and other disorders. *Nature Reviews Neuroscience*, **12**(12): 723–738.